Acta Crystallographica Section D
Biological Crystallography
ISSN 0907-4449

High-resolution structures of oxidized and reduced thioredoxin reductase from *Helicobacter pylori*

Tomas N. Gustafsson,[a]‡ Tatyana Sandalova,[b]*‡ Jun Lu,[a] Arne Holmgren[a] and Gunter Schneider[b]

[a]The Medical Nobel Institute for Biochemistry, Department of Medical Biochemistry and Biophysics, Karolinska Institutet, S-171 77 Stockholm, Sweden, and [b]Division of Molecular Structural Biology, Department of Medical Biochemistry and Biophysics, Karolinska Institutet, S-171 77 Stockholm, Sweden

‡ These authors made equal contributions.

Correspondence e-mail: tatyana.sandalova@ki.se

Received 23 April 2007
Accepted 29 May 2007

PDB References: *H. pylori* TrxR, reduced, 2q0l; oxidized, 2q0k.

The crystal structures of homodimeric thioredoxin reductase (TrxR) from the gastric pathogen *Helicobacter pylori* in complex with $NADP^+$ have been determined for the oxidized and reduced form of the enzyme at 1.7 and 1.45 Å resolution, respectively. The enzyme subunit is built up of FAD- and NAD(P)H-binding domains, each of which contain variants of the Rossmann fold typical of nucleotide-binding proteins. The majority of the amino-acid residues binding the cofactors FAD and NAD(P)H are conserved in the low-molecular-weight thioredoxin reductases. In the reduced species the isoalloxazine ring of FAD is bent along an axis passing through the N5 and N10 atoms with an angle of 22° and the ribityl moiety adopts an unusual conformation. Well defined electron density shows the position of the whole $NADP^+$ molecule with a binding mode similar to that observed in the *Escherichia coli* TrxR–thioredoxin complex, although the orientation of the NAD(P)H-binding domain is different. Rigid-body rotation of this domain to the orientation observed in the *E. coli* TrxR–thioredoxin complex positions $NADP^+$ adjacent to the FAD molecule, suitable for electron transfer, without any readjustments of the conformation of $NADP^+$. A comparison of the binding surfaces of thioredoxin and thioredoxin reductases from *H. pylori* and *E. coli* shows that the overall surface charge distribution in these proteins is conserved and that residue substitutions that change the shape of the binding surface may account for the species-specific recognition of thioredoxin by TrxR.

1. Introduction

The gastric pathogen *Helicobacter pylori* is the main aetiological agent in peptic ulcer disease and type B gastritis and has been classified as a definite carcinogen by the World Health Organization owing to its strong correlation with gastric carcinoma and gastric lymphoma (Suerbaum & Michetti, 2002). It has been estimated that half of the world population is infected, with frequencies ranging from 20 to 80% and showing a clear correlation with low developmental and socioeconomic status (Kusters *et al.*, 2006; Bjorkholm *et al.*, 2003). Like many other pathogens, *H. pylori* shows increasing resistance towards commonly used antibiotics, which gives rise to concerns about future capabilities for clinical treatment (Calvet, 2006). Therefore, there is an obvious need to characterize new antibacterial targets in *H. pylori*.

Colonization of the host by *H. pylori* often results in a strong inflammatory response, with a massive production of reactive oxygen species (Matthews & Butler, 2005). Although *H. pylori* is a microaerophile that requires low oxygen tension

for *in vitro* cultivation, it is able to withstand this onslaught and establish persistent infections. Several different enzymatic activities are responsible for protection against these conditions, some of which are thioredoxin-dependent (Wang *et al.*, 2006).

Thioredoxin (Trx), a widely expressed 12 kDa protein, is a key participant in several crucial cellular pathways (Holmgren, 1985). Trx contains two active-site cysteine residues that transfer electrons to the substrate, generating a disulfide. Thioredoxin is in turn reduced by thioredoxin reductase, which together with NADPH makes up the thioredoxin system (Holmgren & Björnstedt, 1995; Arner & Holmgren, 2000). The thioredoxin system is present in all organisms so far investigated and in most cases is complemented by the glutathione/glutaredoxin system (Fernandes & Holmgren, 2004). Reduced thioredoxin is an electron donor for ribonucleotide reductase, protein methionine sulfoxide reductase and thioredoxin-dependent peroxidases (Ritz & Beckwith, 2001; Kondo *et al.*, 2006; Lillig & Holmgren, 2007).

Unlike other bacteria, *H. pylori* lacks glutathione and glutathione-dependent enzymes such as glutaredoxins (Fahey, 2001). However, in the *H. pylori* genome there are two genes encoding thioredoxins and one gene encoding a thioredoxin reductase (Baker *et al.*, 2001), suggesting a strong dependence on the thioredoxin system for reduction of the essential enzyme ribonucleotide reductase and protection against oxidative stress.

Thioredoxin reductase (TrxR; EC 1.6.4.5) is a member of the pyridine nucleotide–disulfide oxidoreductase family (Luthman & Holmgren, 1982; Holmgren & Björnstedt, 1995; Williams *et al.*, 2000). Enzymes belonging to this family, for example TrxR (Kuriyan *et al.*, 1991), glutathione reductase (GR; Karplus & Schulz, 1989), lipoamide dehydrogenase (Mattevi *et al.*, 1992), trypanothione reductase (Zhang *et al.*, 1996) and mercuric ion reductase (Schiering *et al.*, 1991), are characterized by a common fold, a redox-active disulfide bond and a tightly bound FAD molecule. The members of this family reduce disulfide bonds in many different substrates, catalyzing electron transfer from NAD(P)H *via* a flavin to a disulfide-containing substrate. The TrxRs present in prokaryotes, yeast and plants differs from other members of the family (including GR and mammalian TrxR) in several aspects: they lack the interface domains that are responsible for dimerization in other proteins belonging to this family and the active disulfide is located at different regions of the chain. Furthermore, a large rotation of one domain in low-molecular-weight TxrRs is necessary for completion of the catalytic cycle (Lennon *et al.*, 2000), in contrast to the mechanism of the larger mammalian enzymes (Zhong *et al.*, 2000; Sandalova *et al.*, 2001; Biterova *et al.*, 2005).

All plant and microbial TrxRs have subunits of MW 33–37 kDa, in contrast to 55 kDa or larger for the mammalian TrxRs. Three-dimensional structures of low-molecular-weight TrxRs from three different organisms have been published: those from *E. coli* (Kuriyan *et al.*, 1991; Waksman *et al.*, 1994), *Arabidopsis thaliana* (Dai *et al.*, 1996) and *Mycobacterium tuberculosis* (Akif *et al.*, 2005). The alignment of the amino-acid sequence of *H. pylori* TrxR with that of TrxRs of known three-dimensional structure shows 35–37% identity, suggesting that the overall folds of these proteins are the same.

Here, we report the three-dimensional structure of wild type *H. pylori* thioredoxin reductase complexed with $NADP^+$ as the oxidized and sodium dithionite-reduced species. The crystal structure analysis provides insights into the architecture of the active site and forms the basis of a comparison to other members of the low-molecular-weight TrxR subfamily.

2. Experimental procedures

2.1. Protein production

E. coli strain BL21(DE3) *TrxB*$^-$ (with chromosomal inactivation of the gene coding for *E. coli* thioredoxin reductase) was transformed with the plasmid pPROK/TR harbouring the gene (HP0825) encoding *H. pylori* thioredoxin reductase from strain 26695 (Baker *et al.*, 2001). Large-scale production was performed in 20 l fermentor format, in which the cells were grown to an OD_{600} of 0.7 at 310 K in standard LB medium. Gene expression was induced with 1 m*M* IPTG for 5 h at 310 K, after which the cells were harvested, frozen and disrupted using a French press.

2.2. Protein purification

A 10.5 g cell pellet (equivalent to 5 l culture) was thawed and resuspended in 120 ml 50 m*M* Tris buffer pH 8.0 containing 1 m*M* EDTA, 0.1 m*M* FAD, 0.1 mg ml^{-1} lysozyme, 4 µg ml^{-1} DNAse I, 1 m*M* PMSF and two Complete EDTA-free protease inhibitor tablets (Roche). The lysate was sonicated on ice, cleared by centrifugation for 1 h at 20 000*g* and precipitated with 80% $(NH_4)_2SO_4$. The slurry was centrifuged for 90 min at 20 000*g*, the pellet was resuspended in 50 ml 50 m*M* Tris–HCl pH 8.0, 1 m*M* EDTA (buffer *A*), centrifuged again for 1 h at 20 000*g* and desalted using a G25 Sephadex column equilibrated with the same buffer. The desalted solution was loaded onto a DEAE-Sephacel column (120 ml) equilibrated with buffer *A*, washed with one column volume of buffer *A* followed by several column volumes of 50 m*M* Tris–HCl pH 7.5, 1.0 m*M* EDTA (buffer *B*) and eluted using buffer *B* by increasing the concentration of NaCl stepwise from 50 to 200 m*M*. After elution, the protein was directly loaded onto a 2′,5′-ADP-Sepharose column (35 ml bed volume) equilibrated with buffer *B*, washed with several column volumes of buffer *B*, increasing the concentration of NaCl stepwise to 200 m*M*, and eluted using the same buffer by a stepwise increase of the salt concentration to 1.0 *M*. The purest fractions as judged by visual inspections of Coomassie-stained SDS–PAGE were concentrated to 20 mg ml^{-1} and separated on a pre-packed 16/60 Superdex 200 gel-filtration column equilibrated with 50 m*M* Tris–HCl pH 7.7, 1 m*M* EDTA at a flow rate of 0.5 ml min^{-1}. The purest fractions were pooled, concentrated to about 30 mg ml^{-1} and stored at 277 or 193 K until further use. Typically, 15–20 mg electrophoretically pure protein was obtained per litre of culture.

Table 1
Data-collection and refinement statistics of TrxR from *H. pylori*.

Values in parentheses are for the highest resolution shell.

	Oxidized	Reduced
Data collection		
Resolution (Å)	64.0–1.7 (1.79–1.70)	64.0–1.45 (1.53–1.45)
Space group	$P2_1$	$P2_1$
Unit-cell parameters		
a (Å)	50.1	50.4
b (Å)	99.2	99.4
c (Å)	64.4	64.8
β (°)	100.0	97.9
No. of reflections		
Observed	237222	370050
Unique	66999	105645
$\langle I/\sigma(I)\rangle$	16.6 (2.1)	18.0 (4.0)
Completeness (%)	98.4 (90.1)	94.5 (69.7)
$R_{\rm merge}$ (%)	5.9 (42.9)	5.7 (19.5)
No. of monomers per ASU	2	2
Solvent content (%)	48	48
B factor from Wilson plot (Å^2)	25.0	14.5
Refinement statistics		
$R_{\rm cryst}$ (%)	18.8	16.9
$R_{\rm free}$ (%)	22.6	19.4
No. of atoms with occupancy > 0		
Total	5249	5521
Protein	4690	4789
FAD	106	106
NADP$^+$	96	96
Solvent	357	530
B factors (Å^2)		
Average	29.4	16.5
Protein main chains	28.2	14.4
Protein side chains	30.1	16.9
FAD	21.2	10.8
NADP$^+$	21.3	20.1
Solvent	38.2	25.8
R.m.s.d. from ideal geometry		
Bond lengths (Å)	0.011	0.008
Bond angles (°)	1.60	1.48
Ramachandran plot		
Residues in most favoured regions (%)	90.0	90.0
Residues in disallowed regions (%)	0.0	0.0

2.3. Crystallization

4 µl protein solution (10–15 mg ml^{-1} enzyme in 50 m*M* Tris–HCl, 1 m*M* EDTA pre-incubated with 15 m*M* NADP$^+$ and 30 m*M* $MgCl_2$ for 30 min) was mixed with 1 µl 71 m*M* pentaethylene glycol monooctyl ether or 80 m*M* CHAPSO and 4 µl well solution containing 20–25% PEG 1500, 100 m*M* MIB buffer composed of malonic acid, imidazole and boric acid (Newman, 2004) pH 6.0 in sitting-drop plates and the drops were allowed to equilibrate for 2–3 d, after which streak-seeding was performed. Crystals usually appeared after 2–5 d and grew to full size in 2–4 weeks. The best diffracting crystals were generally obtained after two or three rounds of streak-seeding and grew as bright yellow rods.

2.4. Crystallographic data collection

X-ray data were collected at a temperature of 100 K and a wavelength of 0.9393 Å at the synchrotron beamline ID23-1, ESRF, Grenoble to 1.45 Å resolution for reduced TrxR and 1.7 Å resolution for the oxidized enzyme. In order to prepare reduced TrxR, crystals were briefly soaked in crystallization buffer containing 35% PEG 1500 for cryoprotection and 100 m*M* sodium dithionite. X-ray data were processed with *MOSFLM* (Leslie, 1992) and scaled using the program *SCALA* from the *CCP*4 suite (Collaborative Computational Project, Number 4, 1994). The statistics of the data sets are given in Table 1. The crystals belong to the monoclinic space group $P2_1$, with unit-cell parameters a = 50.1, b = 99.2, c = 64.4 Å, β = 100.0° for oxidized TrxR and a = 50.4, b = 99.4, c = 64.8 Å, β = 97.9° for reduced TrxR. Estimation of the solvent content suggested that the asymmetric unit is most likely to contain a dimer (Mathews coefficient = 2.38 Å^3 Da^{-1}).

2.5. Molecular replacement and crystallographic refinement

Molecular replacement was carried out using the program *MOLREP* (Vagin & Teplyakov, 1997). Of the members of the bacterial pyridine nucleotide–disulfide oxidoreductase family of known three-dimensional structure, the amino-acid sequence of *H. pylori* TrxR is most similar to those of the enzymes from *M. tuberculosis* (37% identity) and *E. coli* (35%). A polyserine model of a monomer of *E. coli* TrxR (PDB code 1tde) was generated and used as a search model for the data set collected from the oxidized TrxR crystal. The calculations resulted in two solutions above all others, giving one dimer in the asymmetric unit with R = 54.4% and perfect crystal packing. The next best solution had an R value of 59%.

The coenzyme FAD was excluded from the search model and the correctness of the molecular-replacement solution was confirmed by electron density for FAD appearing at the expected positions. Refinement of oxidized TrxR was performed with *REFMAC*5 (Murshudov *et al.*, 1997) and 5% of the data were selected in order to monitor the progress of the refinement by the calculation of $R_{\rm free}$. The first rounds of restrained refinement with tight NCS restraints resulted in a decrease of $R_{\rm free}$ from 50.4% to 44.3%. Later during refinement, medium NCS restraints were used. Manual rebuilding of the model was performed using the programs *O* (Jones *et al.*, 1991) and *Coot* (Emsley & Cowtan, 2004). The program *ARP*/*wARP* (Morris *et al.*, 2003) was used to fit the sequence of the *H. pylori* TrxR to the electron-density map. The 2′-phospho-AMP moiety of NADP$^+$ was easily modelled in strong positive difference electron density (>4σ) observed at the expected binding sites in both subunits, whereas electron density for the whole NADP$^+$ molecule is only clearly seen in subunit *A*. Water molecules were added based on peak heights, shape of the electron density, temperature factors and capability to form hydrogen bonds to surrounding protein residues and/or other water molecules. Isotropic individual *B*-factor refinement was employed throughout. At the end of the refinement procedure, several cycles of TLS refinement were carried out. Every subunit was divided into 12 TLS groups as suggested by the TLS Motion Determination server (Painter & Merritt, 2006).

Refinement of reduced TrxR was initiated with five cycles of rigid-body refinement with the fully refined oxidized TrxR as

the starting model. These steps were followed by several cycles of restrained refinement using *REFMAC*5 interspersed with manual adjustment of the model. After refinement using the protocol outlined above (except for the TLS refinement step) had converged, the NCS restraints were removed, resulting in a fall in $R_{\rm free}$ of 3.0%. In the very last steps, restrained anisotropic atomic displacement parameters (ADP) refinement without noncrystallographic symmetry restraints was used. The refinement and final model statistics for reduced and oxidized TrxR are shown in Table 1.

During refinement, the protein model was analyzed using *MOLPROBITY* (Davis *et al.*, 2004) in order to monitor the stereochemistry. A model of *H. pylori* thioredoxin (Trx1) was created using the SwissProt modelling server (Schwede *et al.*, 2003) and the coordinates of *E. coli* Trx (Lennon *et al.*, 2000). Analysis of the dimer interface was performed using the PISA server (Krissinel & Henrick, 2005). Atomic structure representations were generated using *PyMOL* (DeLano, 2002) and surface representations were made using *GRASP* (Nicholls *et al.*, 1991).

3. Results and discussion

3.1. Electron-density map and quality of the model

The structures of TrxR from *H. pylori* were refined in the oxidized and reduced forms to 1.7 and 1.45 Å resolution, respectively. The polypeptide chain (a total of 311 residues) for both subunits of the dimer is well defined in the electron-density maps, except for the C-terminal histidine residue and the very mobile loop comprising residues 34–36. The final models include residues 1–311 of both subunits for reduced and oxidized TrxR. For several residues of the 1.45 Å model alternative conformations were suggested by the electron-density map and were modelled accordingly. The FAD molecules are very well defined in the electron density in both forms of TrxR (Fig. 1). $NADP^+$ molecules could be modelled in both subunits of the reduced TrxR and in subunit *A* of the oxidized enzyme. In subunit *B* of the oxidized enzyme only the 2′-phospho-AMP moiety of the $NADP^+$ was refined with full occupancy and the occupancy of the nicotinamide ring was set to 0.5. The stereochemistry of the model is good (Table 1), with 90% of the residues within the most favourable Ramachandran regions.

3.2. Overall structure of *H. pylori* TrxR

The overall structure of *H. pylori* TrxR is very similar in both forms; superposition of the reduced and oxidized enzyme results in an r.m.s.d. value of 0.8 Å for 612 C^α atoms. The asymmetric unit of the crystal contains a dimer of TrxR. The last steps of crystallographic refinement were carried out without noncrystallographic symmetry restraints for the high-resolution data set (Table 1). Despite the independent refinement of the two subunits, their backbones are rather similar, with an r.m.s.d. of 0.53 Å for all amino acids when the two subunits of reduced TrxR are superimposed. Several loop regions show slightly different conformations, with the largest shift of 2 Å found for residue 211. However, the overall structure is very similar and the following description of the TrxR structure and the active-site architecture is valid for all subunits until indicated otherwise.

The subunit of the *H. pylori* enzyme as well as that of other low-molecular-weight TrxRs consists of two domains: the FAD-binding domain (residues 1–115 and 239–311) and the NAD(P)H-binding domain (residues 116–238) (Figs. 2*a* and 3). The two domains of the subunit are separated by a large cleft filled with solvent molecules and there are only a few contacts between protein atoms from these two domains. The structural cores of the FAD- and NAD(P)H-binding domains are both variants of the Rossmann fold, with each domain containing two β-sheets, a central five-stranded parallel β-sheet and a three-stranded β-meander which is packed against the larger β-sheet (Fig. 2*a*). The other side of the parallel sheet is covered by several α-helices. These nucleotide-binding domains bind NAD(P)H and FAD in a manner

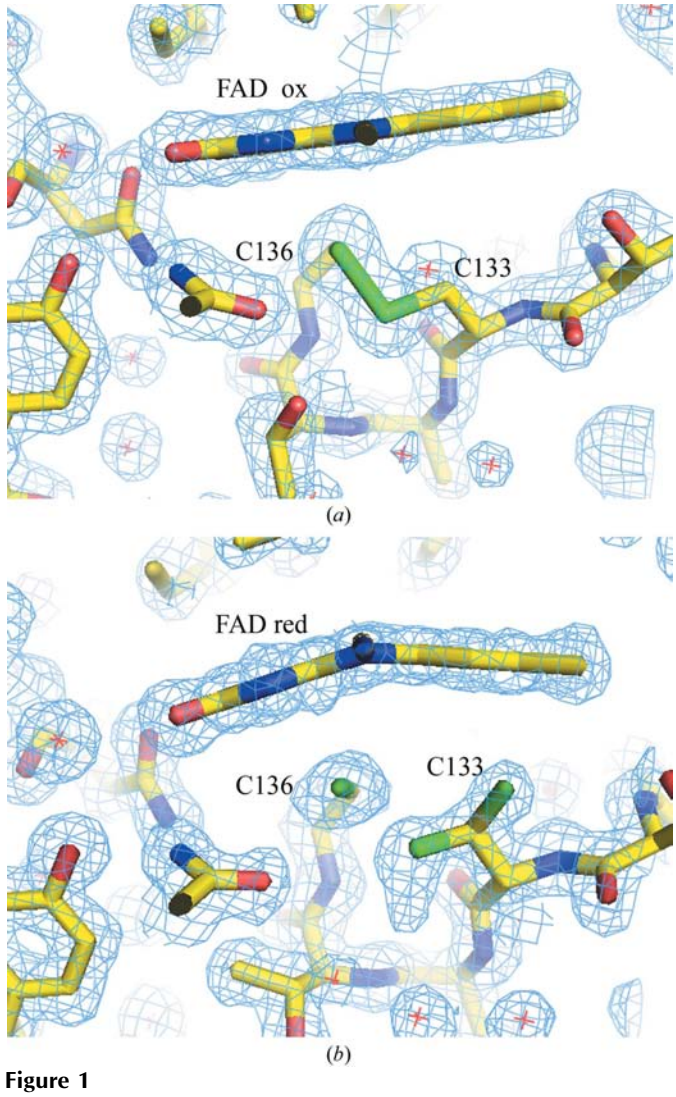

Figure 1
Electron-density maps. Parts of $2F_o - F_c$ OMIT maps at the active site of oxidized (*a*) and reduced (*b*) *H. pylori* TrxR contoured at 1.3σ. The refined models of oxidized and reduced TrxR are superimposed. Both conformations of the side chain of Cys133 in reduced TrxR are shown.

that is characteristic of this fold (Karplus & Schulz, 1989). The redox-active disulfide of *H. pylori* TrxR is located in the NADP(H)-binding domain as in all low-molecular-weight TxrRs (Kuriyan *et al.*, 1991). Similar to other proteins with the Rossmann fold, the active site is located at the C-terminus of the central β-sheet. Residues from the loops that connect β-strands to the following helices are the main building blocks of the active site. Loop β8–α4 contains the first active-site cysteine residue **Cys133** [here and in the following residues that are conserved in low-molecular-weight TrxRs (Fig. 3) are shown in bold] and the second, **Cys136**, is situated in helix α4.

The relative orientation of the FAD- and NAD(P)H-binding domains differs in the FO and FR conformations of *E. coli* TrxR (Lennon *et al.*, 2000). In the FO state (allowing flavin oxidation by the disulfide), the orientations of the NAD(P)H and FAD domains are such that the nicotinamide ring of NADPH is located very far from the FAD molecule and the active-site disulfide is buried between the domains and is non-accessible to water molecules (and even less so to the bulky thioredoxin). A large rotation of the NAD(P)H-binding domain brings the nicotinamide ring close to the isoalloxazine and exposes **Cys133** for reaction with the substrate. This conformation has been called the FR state since it allows flavin reduction by NADPH (Lennon & Williams, 1996). It is worth emphasizing that the FO and FR conformations differ in the domain arrangement rather than the redox state of the protein. Both the structures described here are in the FO conformation independently of the state of the active-site redox centres.

3.3. Dimer interface

H. pylori TxrR is found as a homodimer both in solution and in the crystal, with a dimerization mode that differs from that of the GR-type oxidoreductases. In GR-like proteins the interface domain is mostly responsible for the dimerization and the active sites are located at the interface between the two subunits. The interface domain is absent in low-molecular-weight TrxRs and the FAD-binding domain of subunit *A* makes contacts with both domains of subunit *B*. Owing to the large rotation of one of the domains, the interface differs between the FO and FR states of the protein. In the FO state the subunit–subunit interface contains two parts: a larger part between the FAD domains of both subunits and a smaller part which covers 400 Å^2 between the FAD domain of one subunit and the NADP(H) domain of another. The whole inter-subunit buried surface area is about 2200 Å^2, which is 15% of the fully accessible surface area of the subunit. The majority (63%) of the interface residues are nonpolar, but 19 hydrogen bonds also contribute to the subunit–subunit interactions. Another interaction area is formed by residues of the NAD(P)H domain in the vicinity of the active-site disulfide and the last C-terminal helix α7. Of the 14 residues that form inter-subunit hydrogen bonds in *H. pylori* TrxR, seven are conserved in other low-molecular-weight TrxRs and a further five have conserved substitutions (Fig. 3). A central role in the formation of the dimer interface of the FO state is taken by the invariant **Arg22** (Fig. 2*b*). The side chain of this residue participates in four hydrogen bonds with amino acids from the other subunit. Two of them ensure the specific conformation of the **Arg22** guanidinium group, interacting with the side chain of the invariant residue **Glu47** (NE···OE1,

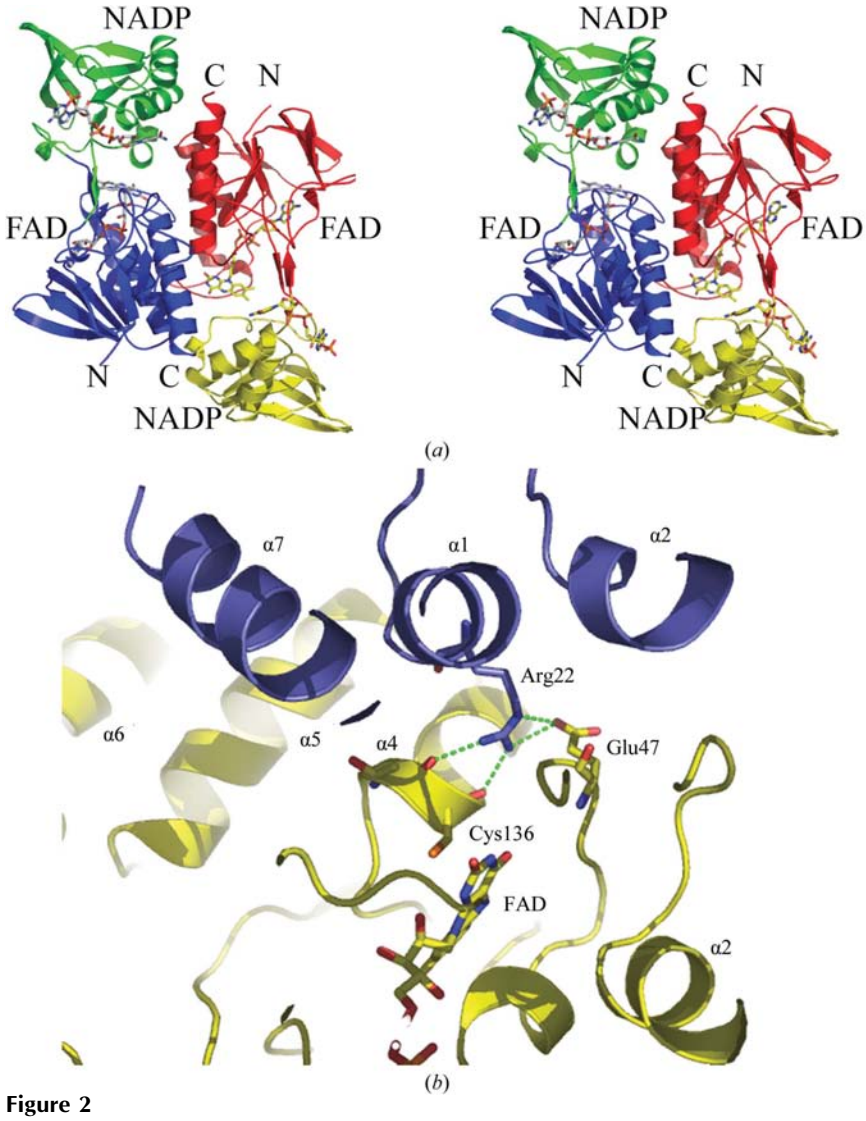

Figure 2
(*a*) Stereo ribbon representation of the dimer of *H. pylori* thioredoxin reductase. Bound FAD and NADP$^+$ are shown in stick representation. Subunits are coloured by domain organization, with the FAD-binding domains in blue and red and the NAD(P)H-binding domains in yellow and green. (*b*) Interactions of the conserved residue Arg22 in the dimer interface of TrxR of *H. pylori*. The two subunits are indicated in different colours.

NH2···OE1). Two other hydrogen bonds are formed with the main-chain O atoms O135 and O136, creating a distortion of the short helix 134–141 that contains **Cys136**, the active-site cysteine residue closest to the flavin.

3.4. Comparison with related enzymes

Three-dimensional structures of low-molecular-weight TxrR from three different organisms have been determined to date: several structures of *E. coli* TrxRs (Kuriyan *et al.*, 1991; Waksman *et al.*, 1994; Lennon *et al.*, 1999, 2000) and TrxR from *A. thaliana* (Dai *et al.*, 1996) and from *M. tuberculosis* (Akif *et al.*, 2005). *E. coli* oxidized TrxR was refined to 2 Å resolution and all others to resolutions of 2.5 Å (PDB codes 1clo and 1vdc) and 3 Å (PDB codes 1f6m and 2a87). Thus, the structures of *H. pylori* TrxR are the highest resolution structures of low-molecular-weight TrxRs determined to date.

Low-molecular-weight TrxRs share 35–37% identical residues and superposition of their three-dimensional structures shows that their overall fold and dimerization mode are rather similar, giving r.m.s.d. values of 1.3–1.4 Å for superposition of the monomers and about 1.5 Å for the dimers. Fig. 3 shows the structural alignment of the low-molecular-weight TrxRs with known three-dimensional structure together with the secondary structure of *H. pylori* TrxR as determined using the program *TOP3D* (Lu, 2000). The enzyme from *H. pylori* is the shortest TrxR; the polypeptide chains of other members of this family display insertions in the loop regions and at the N- and C-termini. Conserved regions mostly form the cofactor-binding sites or take part in the formation of dimer interfaces.

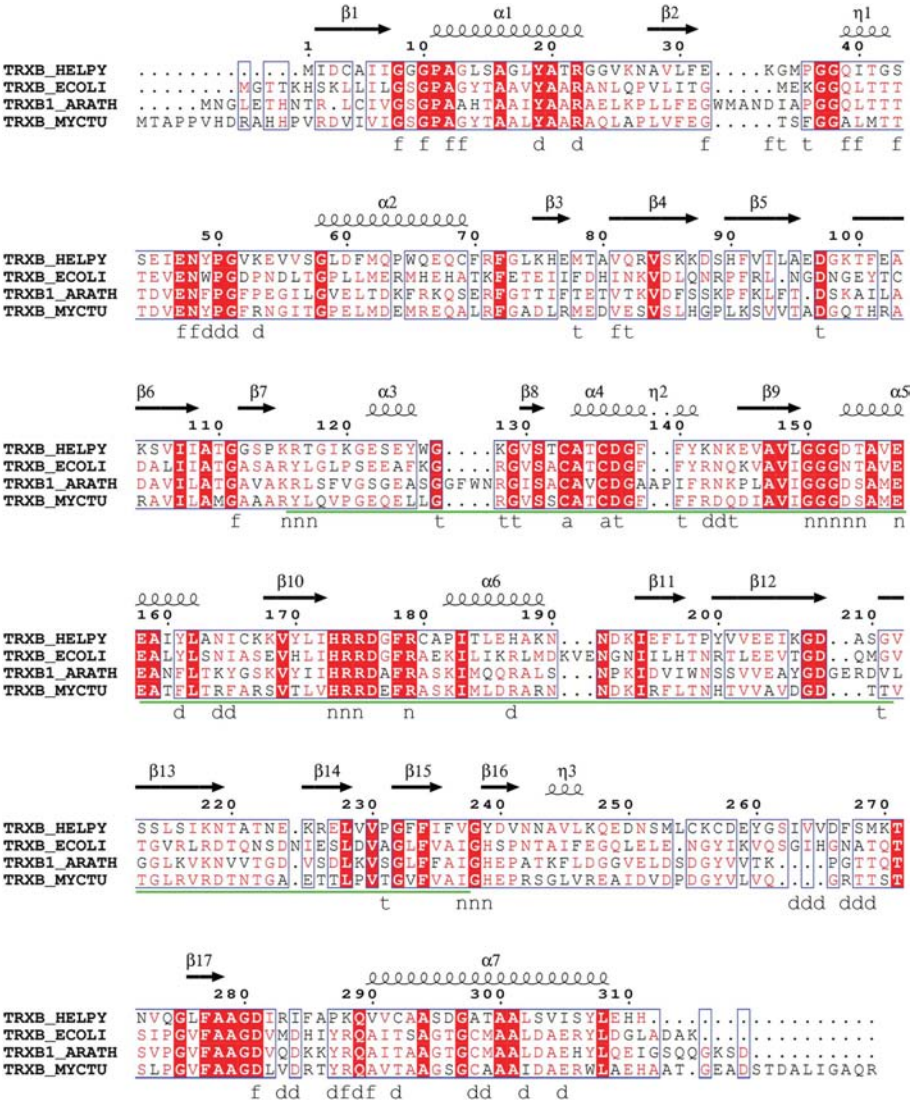

Figure 3
Amino-acid sequence conservation in low-molecular-weight TrxRs. Structural alignment of the sequence of *H. pylori* TrxR with the sequences of three other enzymes from the family: TrxR from *E. coli* (TRXB_ECOLI), *M. tuberculosis* (TRXB_MYCTU) and *A. thaliana* (TRXB1_ARATH). Invariant residues are highlighted by a red background. Residues from the NADP(H)-binding domain are underlined in green. The secondary structure of *H. pylori* TrxR assigned by the program *TOP3D* (Lu, 2000) is shown on the top line. Possible functions of individual residues are indicated on the bottom line [a, catalytically active cysteine residues; f, flavin binding, n, NAD(P)H-binding, d, participation in dimer interface, t, thioredoxin binding]. The figure was produced using the program *MULTALIN* (Corpet, 1988) and the *ESPript* server (Gouet *et al.*, 2003).

3.5. FAD binding in oxidized TrxR

The cofactor FAD is tightly but noncovalently bound to *H. pylori* TrxR. The conformation of the FAD molecule is very similar to that observed in other enzymes belonging to the pyridine nucleotide–disulfide oxidoreductase family. However, the adenine moiety is more accessible to the solvent, a feature that is shared with other low-molecular-weight TrxRs. The isoalloxazine ring of FAD is entirely buried in the interior of the protein and almost all FAD atoms that can act as a hydrogen donor or acceptor are engaged in hydrogen bonds. Many of these interactions between FAD and the enzyme involve conserved residues from the FAD-binding domain and no hydrogen bonds are made to residues located in the NAD(P)H-binding domain (Table 2).

The FAD-binding domain is composed of two parts in the low-molecular-weight TrxRs. The first part of the chain (residues 1–115) binds to atoms from different FAD moieties, while the second half of the FAD domain (residues 228–311) is only close to the FMN moiety of the cofactor. The FAD adenosine packs against the parallel β-sheet in the FAD domain. The adenine ring is located between the side chain of Lys33, which partly shields

Table 2
Interactions of FAD with reduced *H. pylori* thioredoxin reductase.

Hydrogen bonds (cutoff <3.2 Å) and salt bridges (cutoff <3.8 Å) are listed.

FAD atom	TrxR atom	Distance (Å)
Adenine moiety		
N1	Val81 NH	2.9
N3	Lys33 NH	3.3
N6	Val81 CO	2.9
Adenine ribose		
O3*	Glu32 OE1	2.7
O2*	Glu32 OE2	3.0
Pyrophosphate		
OAB	Gln39 NH	2.9
OAC	Gln39 NE2	2.9
OBZ	**Asp281** NH	2.9
OBZ	**Gly111** NH	Water mediated
OBY	**Ala12** NH	3.0
OBY	Gly13 NH	Water mediated
FMN ribityl		
O2′	Lys288 O	2.9
O3′	**Asp281** OD1	2.5
O4′	Ile40 NH	Water mediated
Isoalloxazine		
O2	Val290 NH	2.8
N3	**Asn48** OD1	2.8
O4	**Glu47** NH	Water mediated
N5	Ser43 OG	Water mediated

the adenine from the solvent, and the conserved region **Gly8**–**Gly10**, which allows tight packing although it does not form any hydrogen bonds to the FAD molecule. Both hydroxyl O atoms of the adenosine ribose, O2* and O3*, form hydrogen bonds with the carboxyl group of Glu32. This feature has been found in many nucleotide-binding proteins, including glutathione reductase (Karplus & Schulz, 1989) and lipoamide dehydrogenase (Mattevi *et al.*, 1992), but not in mammalian TrxR, where the replacement of glutamic acid by the shorter side chain of Asp42 only allows the formation of one hydrogen bond to the ribose. However, residue Glu32 is not conserved in low-molecular-weight TrxRs (Fig. 3). In the *E. coli* enzyme a hydrogen bond was found between O2* and Ser9 OG and in the *M. tuberculosis* enzyme O2* and O3* form hydrogen bonds with main-chain atoms (O47 and N50), whereas only water molecules are in contact with the ribose O atoms in -*A. thaliana* TrxR.

With the exception of the hydrogen bond to the side chain of the conserved residue **Gln39**, the O atoms of the diphosphate group interact exclusively with main-chain N atoms (Table 2). The side chains of other residues are not engaged in hydrogen bonds to the diphosphate moiety; nevertheless, this part of the FAD-binding site is one of the most conserved in the enzyme family, suggesting that shape complementarity may be an important determinant in recognition and binding. As in other pyridine nucleotide–disulfide oxidoreductases, there is no positively charged residue in the immediate vicinity of the diphosphate group. The negative charge is compensated through the dipole of helix α1 and two hydrogen bonds to main-chain N atoms. In *H. pylori* TrxR, as well as in GR and lipoamide dehydrogenase, several water molecules participate in a hydrogen-bond network that tethers the diphosphate group to the protein.

The isoalloxazine ring forms fewer hydrogen bonds to TrxR protein atoms than observed in other GR-like proteins. Only two atoms, N3 and O2, make direct hydrogen bonds to protein atoms (Table 2). The O2 atom interacts with the backbone N atom of the N-terminal residue of helix α7, Val290, and forms another water-mediated hydrogen bond to the amide N atom of Val291. These interactions are not only conserved in this enzyme family, including GR (Karplus & Schulz, 1989), but are also found in other flavoenzymes such as *p*-hydroxybenzoate hydroxylase (Schreuder *et al.*, 1994) and phenol hydroxylase (Enroth *et al.*, 1998). This interaction is assumed to stabilize the negative charge at the O2 atom during catalysis (Hol *et al.*, 1978). The N3 atom of the isoalloxazine ring forms a hydrogen bond to the side chain of **Asn48**. Atoms O4 and N5 only form water-mediated hydrogen bonds and their positions and hydrogen-bond distances are the same in both structures of *H. pylori* TrxR.

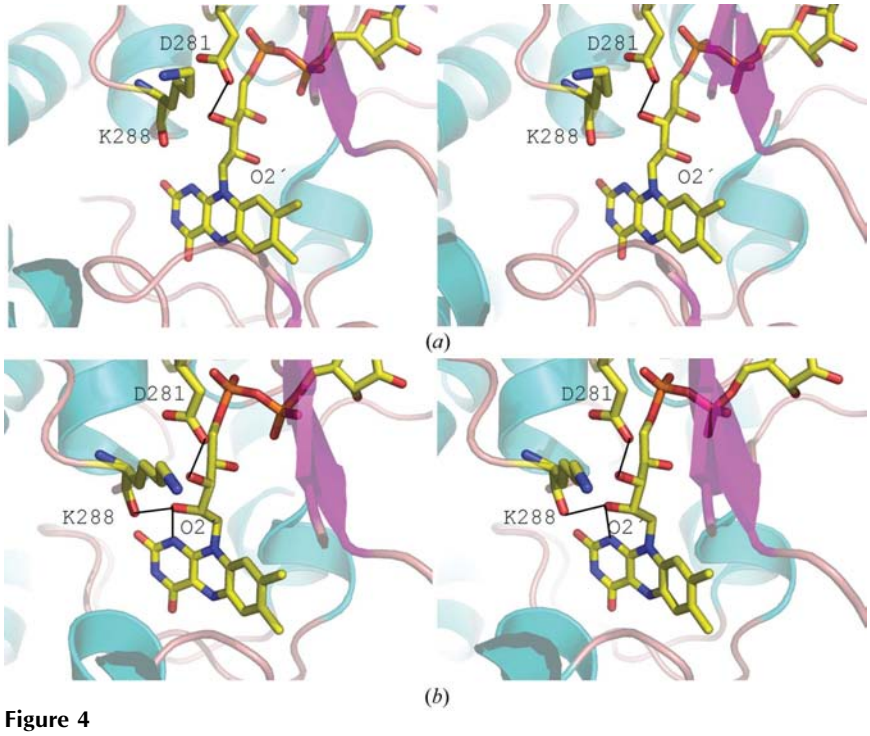

Figure 4
Stereoview of the differences in the hydrogen-bonding interactions of the ribityl moiety of FAD in oxidized (*a*) and reduced (*b*) thioredoxin reductase.

3.6. Structural differences between oxidized and reduced TrxR

In the structure of oxidized TrxR, the isoalloxazine ring is planar (Fig. 1) and the distance between the S atoms of **Cys133** and **Cys136** is about 2 Å, which corresponds to the length of a disulfide bond. **Cys136** S^{γ} is

Table 3
Interactions of $NADP^+$ with reduced *H. pylori* thioredoxin reductase.

Hydrogen bonds (cutoff <3.2 Å) and salt bridges (cutoff <3.8 Å) are listed.

$NADP^+$ atom	TrxR atom	Distance (Å)
Adenine ring		
N3	**Arg174** NH	Water mediated
N6	Thr117 CO	Water mediated
N7	Val237 CO	Water mediated
Adenine ribose		
O3*	**Gly151** NH	3.0
Phosphate of NADP		
OP1	**Arg179** NE	2.9
OP1	**Arg179** NH2	3.2
OP1	**Arg175** NH2	2.8
OP2	**Arg175** NE	2.9
OP2	**Arg174** NE	2.9
OP3	**Arg174** NH2	3.3
OP3	**Arg179** NH2	3.3
Pyrophosphate		
OAB	Asp153 NH	Water mediated
OAC	Lys115 NE	Water mediated
OAC	Tyr239 NH	Water mediated
OAZ	Thr154 NH	3.1
OAZ	Asp153 NH	3.4
OAZ	**Ala155** NH	Water mediated
OAY	Thr154 OG1	3.2
OAY	**Gly238** NH	Water mediated
Nicotinamide ribose		
OBH	Asp153 OD2	2.6
Nicotinamide		
NBO	**Glu157** OE2	3.0

2.9 Å from the C4a atom of FAD, which is suitable for electron transfer between FAD and the disulfide. Addition of sodium dithionite to TrxR results in cleavage of the disulfide bond and reduction of FAD. While the side chain of **Cys136** retains almost the same position as in the oxidized TrxR, the side chain of **Cys133** adopts two alternative conformations in the reduced enzyme (Fig. 1). Reduction of FAD and the active-site cysteine residues has only minor effects on the positions of other amino acids within the active site.

Reduced FAD exhibits a *Re*-face bending of the isoalloxazine ring, resulting in a butterfly-like structure with the outer rings forming the wings (Fig. 1). Atoms N5 and N10 have moved away from the catalytic cysteine residues by 1.2 Å, whereas atoms O2 and C9 are at almost the same positions as in the oxidized species. The bending angle of 22°, which is significantly smaller than the angle of 34° observed in reduced *E. coli* TrxR (Lennon *et al.*, 1999), falls into the range 15–28° suggested from molecular-orbital calculations for reduced free flavins (Dixon *et al.*, 1979).

The conformation of the FMN ribityl moiety differs between the oxidized and reduced proteins (Fig. 4). In oxidized TrxR, the O(2′) hydroxyl group is at a distance of 3.3 Å from the main-chain NH group of Ile40. In the reduced FAD, this group has flipped to the opposite side of the ribityl chain and is at hydrogen-bonding distance to the main-chain carbonyl O atom of Lys288. The O(2′) atom can also serve as an acceptor of a hydrogen bond from the protonated N1 atom in the reduced isoalloxazine ring, an interaction that will stabilize the bent conformation of the isoalloxazine as was suggested for FAD bound to *E. coli* TrxR (Lennon *et al.*, 1999). Unlike the *E. coli* enzyme, the O(3′) hydroxyl group is only marginally affected by this conformational change and the same hydrogen bond to OD1 of the conserved **Asp281** is found in the reduced and oxidized forms of TrxR.

3.7. $NADP^+$ binding

The 2′-phospho-AMP moiety of $NADP^+$ is well defined in all four subunits. However, there is no continuous electron density for the nicotinamide part of $NADP^+$ in subunit *B* in oxidized *H. pylori* TrxR and the occupancies for those atoms were therefore set to 0.5 in the model. Similar disorder of the nicotinamide moiety of $NADP^+$ has also been observed in other pyridine nucleotide–disulfide oxidoreductases (Karplus & Schulz, 1989; Sandalova *et al.*, 2001). In the reduced structure, however, there is well defined electron density for the whole $NADP^+$ molecule (Fig. 5) that allows a reliable determination of the $NADP^+$–TxrR interactions (Table 3). $NADP^+$ binds to *H. pylori* TrxR in a conformation very similar to that of $AADP^+$ observed in the complex of *E. coli* TrxR with thioredoxin (Lennon *et al.*, 2000) despite the fact that the orientation of the NAD(P)H- and FAD-binding domains is different in these two structures. The closest distance between the isoalloxazine and the nicotinamide rings is 17.3 Å.

The adenine moiety is packed close to the inter-domain hinge region, the pyrophosphate binds at the C-terminus of the central β-sheet of the NAD(P)H-binding domain and the nicotinamide ring is located near helix α5. The alignment of various low-molecular-weight TrxRs shows there are three conserved regions that are involved in interactions with the phosphate groups of $NADP^+$. The loop β8–α4 containing the active-site disulfide **Cys133–Cys136** and the loop β9–α5 (residues ^{150}**GGGD**T/S**A**V/M**E**^{157}) bind the pyrophosphate of NADP; residues **Arg174**, **Arg175** and **Arg179** from the loop after β10 tightly interact with the 2′-phosphate group of $NADP^+$.

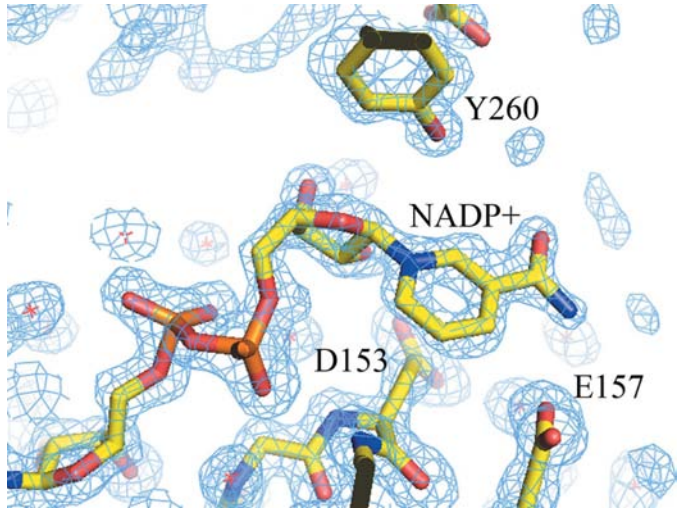

Figure 5
Electron-density map calculated for the final model with $NADP^+$ omitted from the structure-factor calculation. The final model of $NADP^+$ and protein is shown in stick representation.

The adenine ring is bound in a pocket lined with hydrophobic residues and packs with one side against Leu149 and Val237. The other face of the ring system is engaged in a stacking interaction with the guanidinium group of **Arg174** at a distance of 3.4–3.6 Å. None of the adenine atoms form direct hydrogen bonds to the protein. The adenine atom N3 makes two hydrogen bonds *via* water molecules to **His173** NE2 and **Arg174** NH. The N6 and N7 atoms of adenine establish two other water-mediated hydrogen bonds to main-chain atoms of Thr117 and Val237, respectively. The ribose oxygen O3* forms one hydrogen bond to the main-chain N atom of **Gly151**.

TrxR from *H. pylori* is very specific for NADP(H) and cannot utilize NAD(H) (Baker *et al.*, 2001), a property that can be rationalized from the structure. The 2′-phosphate group of NADP(H) forms seven hydrogen bonds/salt bridges to the side chains of three invariant arginine residues, **Arg174**, **Arg175** and **Arg179**, a feature that favours binding of NADP(H) *versus* NAD(H).

Each of the O atoms of the diphosphate moiety of $NADP^+$ forms direct or solvent-mediated hydrogen bonds to protein residues. Most of the bonds are formed by main-chain atoms of the conserved region **Gly152**-**Asp153**-**Thr154**-**Ala155**. Two hydrogen bonds are responsible for the binding and the orientation of the nicotinamide moiety of $NADP^+$ (Table 3). In particular, the interaction between the side chain of **Glu157** and the carboxamide group of the nicotinamide ring appears to be important in maintaining a conformation suitable for catalysis. Tyr260 does not bind to $NADP^+$ directly; however, it is rather close to the nicotinamide ring and partly shields it from the solvent (Fig. 5).

3.8. Thioredoxin-binding site

The structural basis of the binding of thioredoxin by low-molecular-weight TrxRs was first elucidated by crystallographic analysis of the *E. coli* TrxR C135S mutant complexed with the NADP analogue $AADP^+$ and thioredoxin (Lennon *et al.*, 2000). The covalent bond between Cys138 of *E. coli* TrxR and Cys32 of Trx maintains the complex in the FR conformation. NADP(H) is buried between the domains, with the

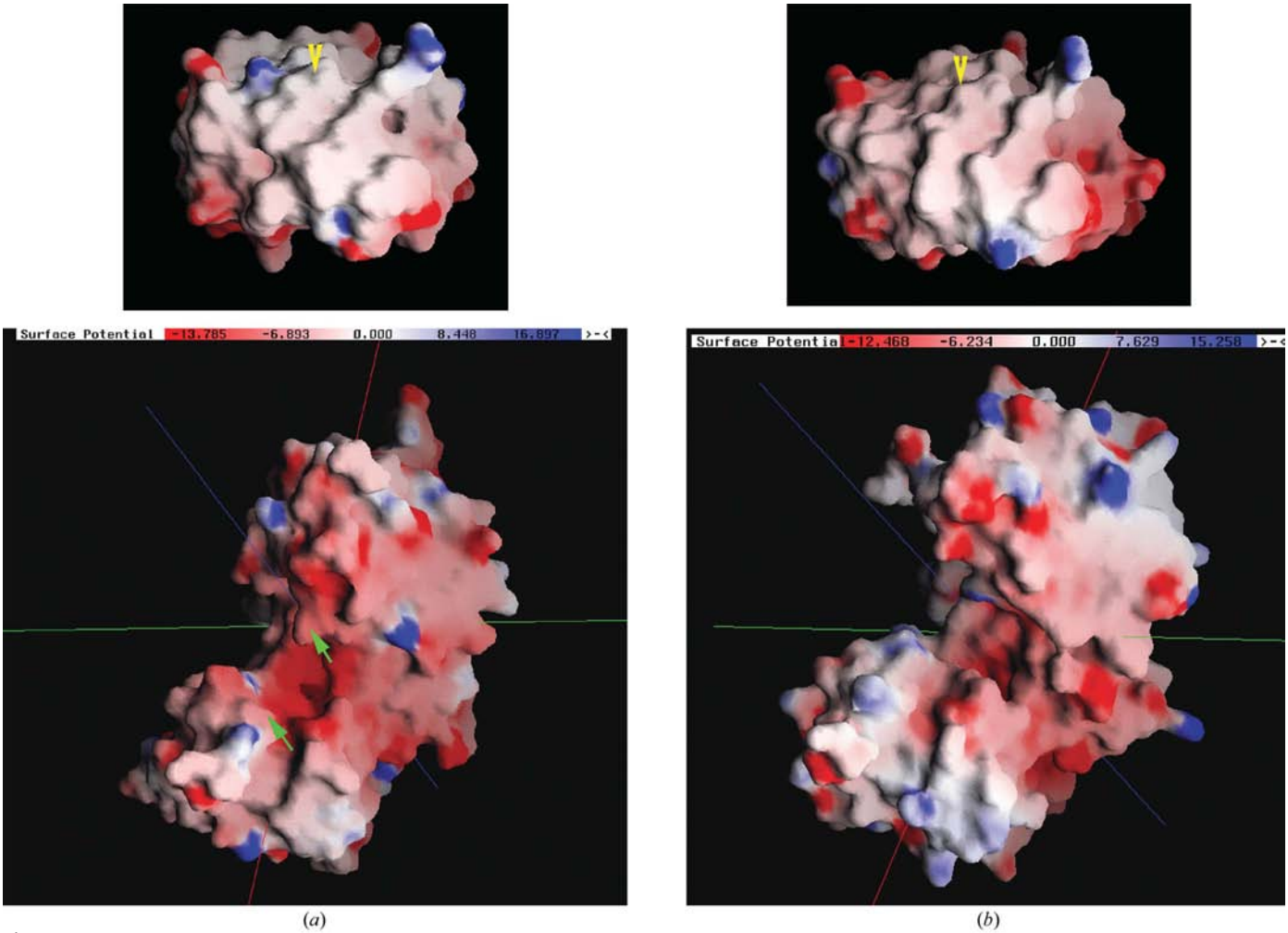

Figure 6
Electrostatic potentials at the interaction surfaces of *E. coli* (*a*) and *H. pylori* (*b*) Trx (upper panel) and TrxR (lower panel). The thioredoxin-binding site of *E. coli* TrxR and the location of the active-site disulfides in Trx are indicated by arrows. The figures were generated using the coordinates of *H. pylori* TrxR and the *E. coli* TrxR–Trx complex (PDB code 1f6m). The coordinates of *E. coli* Trx were also used to construct the homology model of *H. pylori* Trx.

nicotinamide ring packed parallel to the isoalloxazine ring of FAD at a distance of 3.5 Å, suitable for electron transfer (Waksman *et al.*, 1994; Lennon *et al.*, 2000). The active-site cysteine residues are only available for reaction with the substrate in the FR state. The Trx-binding site is composed mostly of helix 4 containing **Cys136** and the loops after β3, β5, β12, β14 and helix 3 (Fig. 3). Six residues of *E. coli* TrxR form hydrogen bonds with Trx: **Asp99**, Asn100, **Gly129**, **Arg130**, **Asp139** and **Phe142**.

It has been shown that *H. pylori* TrxR can reduce thioredoxin from *E. coli*, albeit with lower catalytic efficiency (Baker *et al.*, 2001). The thioredoxin-binding surfaces of the *E. coli* and *H. pylori* TrxRs (Fig. 6) are both characterized by a negative electrostatic potential, with a less negatively charged surface in *H. pylori* TrxR owing to the exchange of Glu38 and Asp82 in *E. coli* TrxR to Met and Thr, respectively. A comparison of the surface-charge distribution of the *E. coli* and *H. pylori* thioredoxins shows that they both have rather acidic surfaces, except for the region that forms the interface in the thioredoxin–thioredoxin reductase complex (Fig. 6). This surface area is predominantly nonpolar, *i.e.* uncharged, and therefore does not show any overall charge complementarity to the negatively charged binding surface in the thioredoxin reductases. Owing to residue substitutions in TrxR at positions Met37 (Gly in *H. pylori* TrxR), His83 (Ala) and Phe80 (Met), the shape of the binding surface differs and these substitutions may account for the species-specific recognition of Trx by TrxR (Baker *et al.*, 2001).

In conclusion, the high-resolution structures of oxidized and reduced thioredoxin reductase from *H. pylori* reported here provide a structural framework for the design and optimization of potent inhibitors with the potential to be developed into new drugs active against this human pathogen.

We acknowledge access to synchrotron radiation at beamline ID23-1, ESRF, Grenoble, France. We thank Alexios Vlamis-Gardikas for the gift of *E. coli* strain BL21(DE3) *TrxB*$^-$ and Leslie B. Poole for the gift of the expression plasmid for *H. pylori* thioredoxin reductase. The work of Björn Elleby in the expression of *H. pylori* TrxR is gratefully acknowledged. This work was supported through grants from the Swedish Research Council.

References

Akif, M., Suhre, K., Verma, C. & Mande, S. C. (2005). *Acta Cryst.* D**61**, 1603–1611.
Arner, E. S. & Holmgren, A. (2000). *Eur. J. Biochem.* **267**, 6102–6109.
Baker, L. M., Raudonikiene, A., Hoffman, P. S. & Poole, L. B. (2001). *J. Bacteriol.* **183**, 1961–1973.
Biterova, E. I., Turanov, A. A., Gladyshev, V. N. & Barycki, J. J. (2005). *Proc. Natl Acad. Sci. USA*, **102**, 15018–15023.
Bjorkholm, B., Falk, P., Engstrand, L. & Nyren, O. (2003). *J. Intern. Med.* **253**, 102–119.
Calvet, X. (2006). *Digestion*, **73**, *Suppl.* 1, 119–128.
Collaborative Computational Project, Number 4 (1994). *Acta Cryst.* D**50**, 760–763.
Corpet, F. (1988). *Nucleic Acids Res.* **16**, 10881–10890.
Dai, S., Saarinen, M., Ramaswamy, S., Meyer, Y., Jacquot, J. P. & Eklund, H. (1996). *J. Mol. Biol.* **264**, 1044–1057.
Davis, I. W., Murray, L. W., Richardson, J. S. & Richardson, D. C. (2004). *Nucleic Acids Res.* **32**, W615–W619.
DeLano, W. L. (2002). *The PyMOL Molecular Graphics System.* http://www.pymol.org.
Dixon, D. A., Lindner, D. L., Branchaud, B. & Lipscomb, W. N. (1979). *Biochemistry*, **18**, 5770–5775.
Emsley, P. & Cowtan, K. (2004). *Acta Cryst.* D**60**, 2126–2132.
Enroth, C., Neujahr, H., Schneider, G. & Lindqvist, Y. (1998). *Structure*, **6**, 605–617.
Fahey, R. C. (2001). *Annu. Rev. Microbiol.* **55**, 333–356.
Fernandes, A. P. & Holmgren, A. (2004). *Antioxid. Redox Signal.* **6**, 63–74.
Gouet, E., Robert, X. & Courcelle, E. (2003). *Nucleic Acids Res.* **31**, 3320–3323.
Hol, W. G., van Duijnen, P. T. & Berendsen, H. J. (1978). *Nature (London)*, **273**, 443–446.
Holmgren, A. (1985). *Annu. Rev. Biochem.* **54**, 237–271.
Holmgren, A. & Björnstedt, M. (1995). *Methods Enzymol.* **252**, 199–208.
Jones, T. A., Zou, J.-Y., Cowan, S. W. & Kjeldgaard, M. (1991). *Acta Cryst.* A**47**, 110–119.
Karplus, P. A. & Schulz, G. E. (1989). *J. Mol. Biol.* **210**, 163–180.
Kondo, N., Nakamura, H., Masutani, H. & Yodoi, J. (2006). *Antioxid. Redox Signal.* **8**, 1881–1890.
Krissinel, E. & Henrick, K. (2005). *Detection of Protein Assemblies in Crystals.* Berlin: Springer-Verlag.
Kuriyan, J., Krishna, T. S., Wong, L., Guenther, B., Pahler, A., Williams, C. H. Jr & Model, P. (1991). *Nature (London)*, **352**, 172–174.
Kusters, J. G., van Vliet, A. H. & Kuipers, E. J. (2006). *Clin. Microbiol. Rev.* **19**, 449–490.
Lennon, B. W. & Williams, C. H. Jr (1996). *Biochemistry*, **35**, 4704–4712.
Lennon, B. W., Williams, C. H. Jr & Ludwig, M. L. (1999). *Protein Sci.* **8**, 2366–2379.
Lennon, B. W., Williams, C. H. Jr & Ludwig, M. L. (2000). *Science*, **289**, 1190–1194.
Leslie, A. G. W. (1992). *Jnt CCP4/ESF–EACBM Newsl. Protein Crystallogr.* **26**.
Lillig, C. H. & Holmgren, A. (2007). *Antioxid. Redox Signal.* **9**, 25–47.
Lu, G. (2000). *J. Appl. Cryst.* **33**, 176–183.
Luthman, M. & Holmgren, A. (1982). *Biochemistry*, **21**, 6628–6633.
Mattevi, A., Obmolova, G., Sokatch, J. R., Betzel, C. & Hol, W. G. (1992). *Proteins*, **13**, 336–351.
Matthews, G. M. & Butler, R. N. (2005). *Helicobacter*, **10**, 298–306.
Morris, R. J., Perrakis, A. & Lamzin, V. S. (2003). *Methods Enzymol.* **374**, 229–244.
Murshudov, G. N., Vagin, A. A. & Dodson, E. J. (1997). *Acta Cryst.* D**53**, 240–255.
Newman, J. (2004). *Acta Cryst.* D**60**, 610–612.
Nicholls, A., Sharp, K. A. & Honig, B. (1991). *Proteins*, **11**, 281–296.
Painter, J. & Merritt, E. A. (2006). *J. Appl. Cryst.* **39**, 109–111.
Ritz, D. & Beckwith, J. (2001). *Annu. Rev. Microbiol.* **55**, 21–48.
Sandalova, T., Zhong, L., Lindqvist, Y., Holmgren, A. & Schneider, G. (2001). *Proc. Natl Acad. Sci. USA*, **98**, 9533–9538.
Schiering, N., Kabsch, W., Moore, M. J., Distefano, M. D., Walsh, C. T. & Pai, E. F. (1991). *Nature (London)*, **352**, 168–172.
Schreuder, H. A., Mattevi, A., Obmolova, G., Kalk, K. H., Hol, W. G., van der Bolt, F. J. & van Berkel, W. J. (1994). *Biochemistry*, **33**, 10161–10170.
Schwede, T., Kopp, J., Guex, N. & Peitsch, M. C. (2003). *Nucleic Acids Res.* **31**, 3381–3385.

Suerbaum, S. & Michetti, P. (2002). *N. Engl. J. Med.* **347**, 1175–1186.
Vagin, A. & Teplyakov, A. (1997). *J. Appl. Cryst.* **30**, 1022–1025.
Waksman, G., Krishna, T. S., Williams, C. H. Jr & Kuriyan, J. (1994). *J. Mol. Biol.* **236**, 800–816.
Wang, G., Alamuri, P. & Maier, R. J. (2006). *Mol. Microbiol.* **61**, 847–860.
Williams, C. H. Jr, Arscott, L. D., Müller, S., Lennon, B. W., Ludwig, M. L., Wang, P.-F., Veine, D. M., Becker, K. & Schirmer, R. H. (2000). *Eur. J. Biochem.* **267**, 6110–6117.
Zhang, Y., Bond, C. S., Bailey, S., Cunningham, M. L., Fairlamb, A. H. & Hunter, W. N. (1996). *Protein Sci.* **5**, 52–61.
Zhong, L., Arner, E. S. J. & Holmgren, A. (2000). *Proc. Natl Acad. Sci. USA*, **97**, 5854–5859.